Modeling and characterization of backside slot LiNbO$_3$ optical modulators

AHMED A. ABOUELFADL[*], FARID S ELHOSARY, ABDULLAH A. ALSHEHRI
Electrical Engineering Department, Faculty of Engineering, King Abdulaziz University, Rabigh 21911, Saudi Arabia

A numerical model of x-cut LiNbO3 optical modulator with backside slot structures to satisfy the velocity matching condition without the layer of silicon dioxide is presented. The analysis of microwave properties of the proposed structures is based on the transverse resonance technique. An equivalent circuit is deduced to represent the structures. Generalized trial quantities are introduced as virtual sources in the equivalent network representation of boundary conditions. The lossy conductor of a planar transmission line is represented by a particular two port network. Thus, the metallic losses can be evaluated for any metallization thickness without restricting the conductor modeling to a simple surface impedance approximation. The dependence of the effective microwave index, the characteristic impedance and the product of the drive voltage and the electrode interaction length on the thickness of substrate near the ground electrode is investigated. The optical response of the modulator is computed. The 3-dB optical bandwidth as a function of substrate thickness is also investigated. These types of modulators are more sufficient for the broadband optical transmission systems up to 40 Gb/s. The obtained results are agreed very well with published practical results and theoretical results of finite element method.

1. Introduction

Advancements in the internet, cellular phones, and multimedia communications have increased the need for large capacity optical transmission systems. The LiNbO$_3$ (LN) modulators with a traveling wave electrode and a Mach-Zehnder optical waveguide is a promising device for high speed systems since the low frequency chirp and wide bandwidth are practicable. Various types of z-cut LN modulators have been developed [1-3]. These structures must have a buffer layer of silicon dioxide for decreasing the microwave index to satisfy the condition of velocity matching and to decrease the optical insertion loss. The buffer layer causes the problem of DC-drift phenomenon [4]. Due to the dielectric nature of the LN, a dc bias voltage applied to the device to adjust the optical output modulation state reduces gradually, resulting in a drift of optical output state. In order to keep the optical output stable, via a feedback loop, the dc bias is cumulatively applied to the device and ultimately will exceed the limitations of the system drivers [5]. X-cut LN optical modulators without buffer layer can suppress this problem, but they have larger driving voltage relative to z-cut modulators of the 50 Ω impedance system [6-7].

A lower driving voltage can be produced by using the back slot structure [8-9]. In this structure, the microwave efficiently leaks into the air around the coplanar waveguide electrode and also the back slot. Therefore, it can satisfy the velocity matching condition between light wave and microwave without the buffer layer. Actually, it was difficult to thin the substrate uniformly and this characteristic of the structure caused the critical problem of

high optical insertion loss. The x - cut LN modulator with a two step back slot structure can be used to achieve low drive voltage and low optical insertion loss.

In this paper, a numerical model of x-cut LN optical modulator with a two step back sand backside slots structures are presented. The analysis is based on the transverse resonance technique [10-11]. The equivalent network of the coplanar line structure is deduced. Generalized trial quantities are introduced as virtual adjustable sources in the equivalent network representation of boundary conditions. The lossy conductor of a planar transmission line is represented by a particular two port network. Thus, metallic losses can be evaluated for all types of electrodes. The optical prosperities of back slot LN optical modulators are characterized.

2. Modeling and characterizing of X-Cut LN optical modulators

2.1 Devices structure

In x-cut LN optical modulator with back slot, the substrate around the optical waveguides has to be uniform thickness comparable to the vertical optical field of the Ti-diffused waveguide. The horizontal mode size remains constant with decreasing thickness but the vertical one decreases because of the stronger confinement, due to the fact that both sides are exposed to air. Thus, the optical field is deformed and the coupling loss with the fiber or optical waveguides that exist on a substrate of a maximum thickness increases. Furthermore, the scattering of the light

wave at the bottom of the fabricated slot occurs, and the propagation loss increases.

To overcome this problem, a two step back slot structure as shown in Fig. 1 is used. In this structure, the thickness T_{LN} of the substrate around the optical waveguide increases to be much larger than the optical mode size in order to avoid the deformation and scattering. The thickness T_{sub} of the substrate near the ground electrodes are thinned for the purpose of decreasing the effective microwave index.
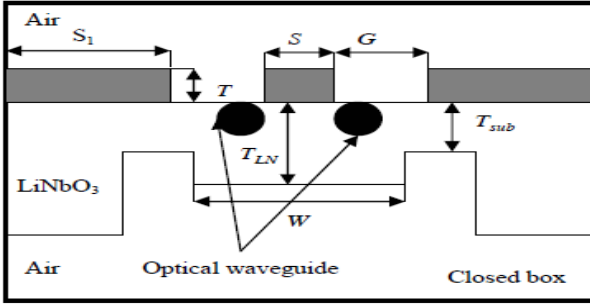

Fig. 1. Cross section of x-cut LN optical modulator.

A second structure x-cut LN modulator with backside slots as in Fig. 2 is considered. Optical 3-dB bandwidth can be increased with x-cut LN substrate when the two slots are incorporated in the structure.
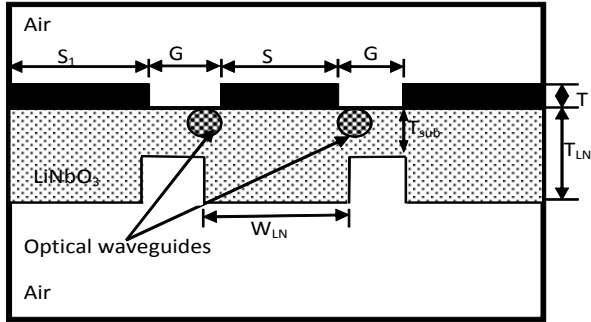

Fig. 2. Cross section of the backside slot LN optical modulator.

2.2 The theoretical performance of modulators

In this section, we study the theoretical performance of the traveling wave type Mach-Zehnder optical modulators of the cross-section shown in Figs.1,2. When we apply an ac modulation voltage of the form:

$$V(z,t) = V_m e^{\alpha z} \cos(\omega t - K_z z) \tag{1}$$

and a dc voltage V_{dc} to the electrode, the optical phase difference at the output end of the modulator, $\Delta\varphi$, is expressed as:

$$\Delta\varphi = \pi \frac{V_{dc}}{V_\pi} + \pi \frac{V_m}{V_\pi} F(f) \sin(\omega t + \varphi) \tag{2}$$

with

$$F(f) = \left[\frac{1 - 2e^{-\alpha L}\cos\theta + e^{-2\alpha L}}{(\alpha L)^2 + (\theta)^2}\right]^{\frac{1}{2}}, \quad \varphi = \tan^{-1}\left[\frac{\alpha L + e^{-\alpha L}(\theta\sin\theta - \alpha L\cos\theta)}{\theta - e^{-\alpha L}(\theta\cos\theta + \alpha L\sin\theta)}\right],$$

$$\theta = \frac{\omega L(N_m - N_o)}{c} \quad and \quad V_\pi . L = \frac{\lambda G}{2\gamma_{33}N_o^3\Gamma}$$

where V_m is the amplitude of the modulation voltage at the input end, α is the attenuation constant, $\omega = 2\pi f$ is the angular frequency of the ac signal, K_Z is the phase conatant of the ac signal, V_π is the half-wave voltage, λ is the light wavelength, G is the gap spacing, γ is the electro-optic coefficient, Γ is the overlap integral between optical and microwave fields, N_o is the effective index of the light signal, L is the coupling length, θ is the difference of the electrical length between optical and signal waves, C is the light velocity in free space, and N_m is the effective index of the signal wave. The optical intensity response can be evaluated as:

$$I = I_o \cos^2\left(\frac{\Delta\varphi}{2}\right) \tag{3}$$

where I_o is the maximum optical intensity response in the absence of modulation voltage i.e. $\varphi = 0$.

The 3-dB optical bandwidth of a traveling-wave modulator can be calculated when the wave velocities are mismatched as:

$$\Delta f = \frac{2c}{\pi|N_o - N_m|L} \tag{4}$$

For a perfect velocity matching condition $N_m = N_o$, the 3-dB optical bandwidth can be determined as:

$$\Delta f = \left(\frac{6.84}{\alpha L}\right) \tag{5}$$

Where α is the total attenuation including both the conductor (α_c) and dielectric (α_d) losses of the modulator structure.

$$\alpha(f) = \alpha_c\sqrt{f} + \alpha_d f \tag{6}$$

2.3 Calculation of the microwave effective index and the characteristic impedance

The microwave effective index N_m can be estimated by using a transverse resonance method where the electrode is treated as a two- port network. The equivalent network of the coplanar line including the two-port network and generalized trial quantities has been deduced as in [10]. Fig. 3 shows the equivalent network used. The microwave effective index is defined as:

$$N_m = \frac{K_z}{K_o} \qquad (7)$$

Where K_z is the microwave propagation constant of the coplanar line and K_o is the free space propagation constant.
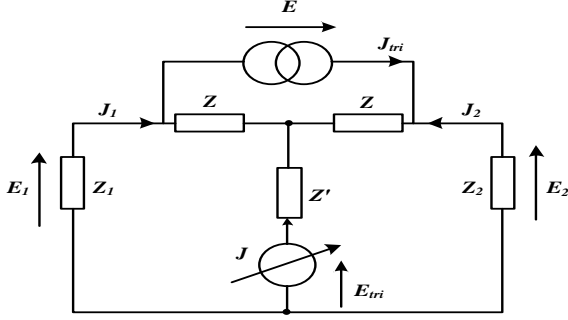

Fig. 3. The equivalent network of the proposed structures.

The solution of the equivalent network gives:

$$\begin{bmatrix} J \\ E \end{bmatrix} = \begin{bmatrix} \hat{H}_{11} & \hat{H}_{12} \\ \hat{H}_{21} & \hat{H}_{22} \end{bmatrix} \begin{bmatrix} E_{tri} \\ H_{tri} \end{bmatrix} \qquad (8)$$

with

$$\hat{H}_{11} = (Z_1 + Z_2 + 2Z)\hat{D}^{-1}$$

$$\hat{H}_{12} = -\hat{H}_{21} = Z(Z_1 + Z_2)\hat{D}^{-1}$$

$$\hat{H}_{22} = 2Z\big(Z_1 Z_2 + (Z_1 + Z_2)(Z' + Z/2)\big)\hat{D}^{-1}$$

where

$$D = (Z_1 + Z)(Z_1 + Z_2 + 2Z)Z', \quad Z_0 = \frac{1+j}{\delta\sigma}, \quad Z' = \frac{Z_0}{\sinh(\gamma_0 T)}, \quad \gamma_0 = \frac{1+j}{\delta}$$

and $Z = Z_0\left[\coth(\gamma_0 T) - \frac{1}{\sinh(\gamma_0 T)}\right]$ and $\delta = \frac{1}{\sqrt{\pi\mu\sigma f}}$

δ and T designate the skin depth and electrode thickness respectively. Z_1 and Z_2 are the impedances of the transmission line layers upper the electrodes and down in the direction of Y. σ is the conductivity of the electrode. Z is the surface impedance.

The trial quantities E_{tri} and J_{tri} do not supply any power into the perfect wall at each side of the modulator structure Figs. 1 and 2. Consequently, one can deduce that

$$\begin{bmatrix} \hat{H}_{11} & \hat{H}_{12} \\ \hat{H}_{21} & \hat{H}_{22} \end{bmatrix} \begin{bmatrix} E_{tri} \\ J_{tri} \end{bmatrix} = 0 \text{ on gaps of electrodes} \qquad (9)$$

This technique is more general with respect to the other techniques where it can be used with thick and thin electrodes. In case of thick electrode the surface impedance Z can be produced, where $Z' = 0$ and $T \gg \delta$, as

$$Z = Z_{thick} = Z_0 \coth(\gamma_0 T) \qquad (10)$$

From Eqs. 8,9 and10, one can deduce that

$$\hat{D}^{-1}\begin{bmatrix} (Z_1 + Z_2 + 2Z_{thick}) & Z_{thick}(Z_1 - Z_2) \\ Z_{thick}(Z_2 - Z_1) & 2Z_{thick}(Z_1 Z_2 + (Z_1 + Z_2)Z_{thick}/2) \end{bmatrix}\begin{bmatrix} E_{tri} \\ J_{tri} \end{bmatrix} = \begin{bmatrix} 0 \\ 0 \end{bmatrix}$$
on gaps of the electrods $\qquad (11)$

where E_{tri} and J_{tri} can be expanded on to sets of trial functions g_p and $h_{p'}$, respectively, which are defined in the entire aperture of the modulator as

$$E_{tri} = \sum_{p=1}^{p} e_p g_p \text{ and } J_{tri} = \sum_{p'=1}^{p'} j_{p'} h_{p'} \qquad (12)$$

with

$$g_{2k-1} = \begin{bmatrix} \Phi_x^{(k)} \\ 0 \end{bmatrix}, g_{2k} = \begin{bmatrix} 0 \\ \Phi_z^{(k)} \end{bmatrix}, h_{2k'-1} = \begin{bmatrix} \Psi_x^{(k')} \\ 0 \end{bmatrix} \text{ and } h_{2k'} = \begin{bmatrix} 0 \\ \Psi_z^{(k')} \end{bmatrix} \qquad (13)$$

The trial functions can be chosen as

$$\begin{cases} \Phi_x^{(k)}(x) = \cos\big((k-1)\pi(x - S_1)/G\big) \\ \Phi_z^{(k)}(x) = \sin\big(k\pi(x - S_1)/G\big) \end{cases} \qquad (14)$$

and

$$\begin{cases} \Psi_x^{(k')}(x) = \sin(k'\pi(x - S_1)/G) \\ \Psi_z^{(k')}(x) = \cos\big((k'-1)\pi(x - S_1)/G\big) \end{cases} \qquad (15)$$

Applying Galerkin's method with cosine trial functions that are shown in equations develops the formal set of integral Eqs.12, 13, 14 and 15 to deduce the following matrix form

$$\sum_n \begin{bmatrix} [(g_p, \hat{H}_{11}g_q)]^{(h,e)} & [(g_p, \hat{H}_{12}h_{q'+p})]^{(h,e)} \\ [(h_{p'+p}, \hat{H}_{21}g_q)]^{(h,e)} & [(g_{p'+p}, \hat{H}_{22}g_{q'+p})]^{(h,e)} \end{bmatrix} = 0 \qquad (16)$$

where $\hat{H}_{11}^{h,e}$, $\hat{H}_{12}^{h,e}$, $\hat{H}_{21}^{h,e}$ and $\hat{H}_{22}^{h,e}$ are functions in $Z_1^{h,e}$ and $Z_2^{h,e}$. $Z_1^{h,e} = (Y_1^{h,e})^{-1}$ and $Z_2^{h,e} = (Y_2^{h,e})^{-1}$. Y_2 is given by $Y_2^{(h,e)} = Y_{n2}^{(h,e)} + Y_{n3}^{(h,e)} + Y_{n4}^{(h,e)}$ of each layer of the structure. Also, the inner product is given by

$$\langle g_p, \hat{H}_{11}g_q \rangle = \sum_n \langle \Phi_x^{(k)}, f_{nx}^{(h,e)} \rangle \hat{H}_{11n}^{(h,e)} \langle f_{nx}^{(h,e)}, \Phi_x^{(k')} \rangle$$

$$f_n^{(h,e)} = \begin{bmatrix} f_{nx} \\ f_{nz} \end{bmatrix}^{(h,e)} = \begin{bmatrix} E_{nx} \\ E_{nz} \end{bmatrix}^{(h,e)}$$

where E_{nx}, E_{nz} are the components of the transverse electric field at Y=0, e and h means TE_y and TM_y, respectively. Y_{n1}, Y_{n2}, Y_{n3} and Y_{n4} are the admittances for the layers of the structure in Y-direction. The basis functions are given as

$$f_{nx}^e = \sqrt{\frac{\sigma_n}{a}} \frac{jK_z}{\sqrt{(K_z)^2 + (n\pi/a)^2}}\cos(n\pi x/a)e^{-jK_z Z},$$

$$f_{nx}^h = \sqrt{\frac{\sigma_n}{a}} \frac{(n\pi/a)}{\sqrt{(K_z)^2 + (n\pi/a)^2}}\cos(n\pi x/a)e^{-jK_z Z},$$

$$f_{nz}^e = \sqrt{\frac{\sigma_n}{a}} \frac{-jK_z}{\sqrt{(K_z)^2 + (n\pi/a)^2}} \cos(n\pi x/a) e^{-jK_z z},$$

and $\quad f_{nz}^h = \sqrt{\frac{\sigma_n}{a}} \frac{-(n\pi/a)}{\sqrt{(K_z)^2 + (n\pi/a)^2}} \sin(n\pi x/a) e^{-jK_z z}$ where

$$\sigma_n = \begin{cases} a & at\ n = 0 \\ \frac{a}{2} & at\ n \neq 0 \end{cases}$$

For certain frequency, Eq. 16 can be solved to calculate the effective microwave index N_m.

The characteristic impedance Z_c can be evaluated as in [10]:

$$Z_c = \frac{V_x^2}{2P} \tag{17}$$

where V_x is the potential distribution between the inner and outer electrodes along x-direction and P is the specfic power wchich cab be evaluated as

$$P = \frac{1}{2} Re\langle \vec{E} | \vec{H} \rangle$$

where E and H are the transverse electric and magnetic fields, respectively.

4. Numerical results

The main target of using the back slots x- cut LN optical modulators is increasing the 3dB- optical bandwidth without the use of the buffer layer. The dependence of the effective microwave index N_m on T_{sub} is illustrated in Fig.4. T_{LN} is fixed at 15μm which must be much larger than the optical mode size. The width of the center electrode S is set to 30μm to decrease the electrode conductor loss. N_m is increased with the increasing of T_{sub}. When the gap G between the center electrode and the ground electrode is in the range from 40-50μm, N_m becomes 2.2 and velocity matching is achieved.
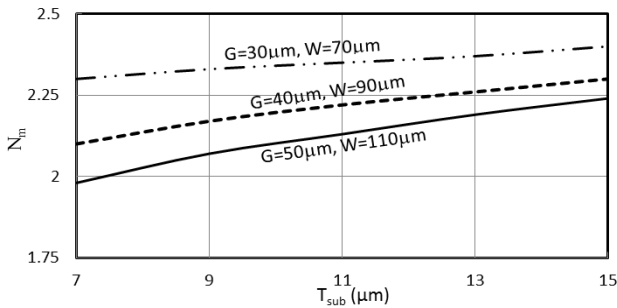

Fig. 4. The dependence of N_m on T_{sub}.

Fig. 5 shows the dependence of the characteristic impedance Z_c on T_{sub}. The characteristic impedance Z_c is decreased with the increasing of the T_{sub}. So, Z_c can be constructed to the 50 Ω impedance system at T_{sub} =15μm
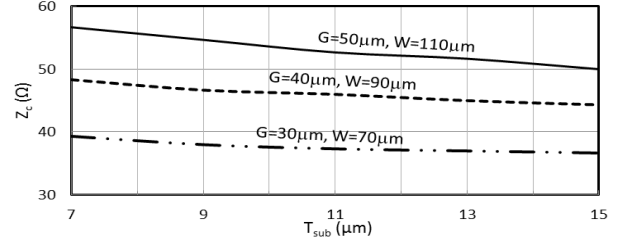
with G=50μm and W=110μm.

Fig. 5. The dependence of Z_c on T_{sub}.

Fig. 6 shows the dependence of the product of the drive voltage V_π and the electrode interaction length L on T_{sub}. $V_\pi L$ becomes 13 V.cm in the case of G = 40 μm. $V_\pi L$ is decreased with increasing T_{sub}. The drive voltage can be reduced to between 2.1 V and 3.2 V, when the electrode interaction length L is between 6 cm and 4 cm which can actually be fabricated.
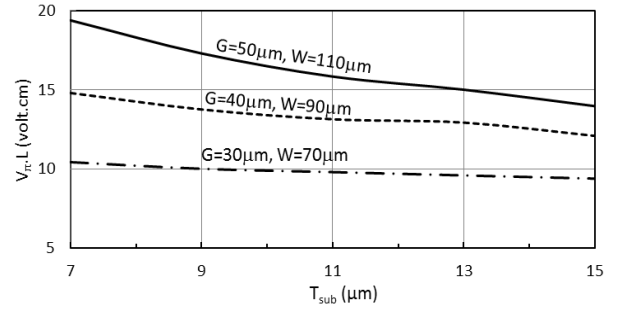

Fig. 6. The dependence of $V_\pi L$ on T_{sub}.

Fig. 7 shows the optical response of the modulator at optical wavelength λ=1.55 μm, V_π =3 V, and $V_\pi L$ = 12 V.cm. The 3 dB bandwidth of the two-step back slot LN optical modulator is equal 27.5GHz.
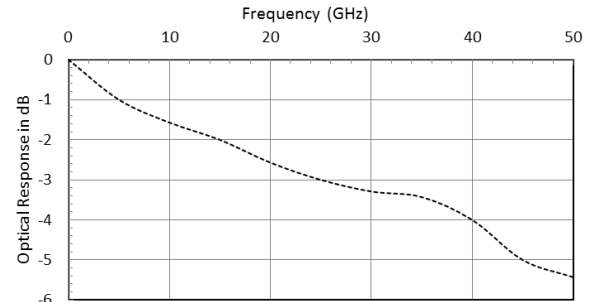

Fig. 7. Optical response as a function of frequency.

Fig. 8 illustrates the variation of the N_m for backside slot x-cut LN modulator of Fig. 2 with the substrate thickness T_{sub}. It is seen that the results agree very well with results of both the finite elements method and the available experiment [12]. The microwave effective index increases with the increase in substrate thickness.
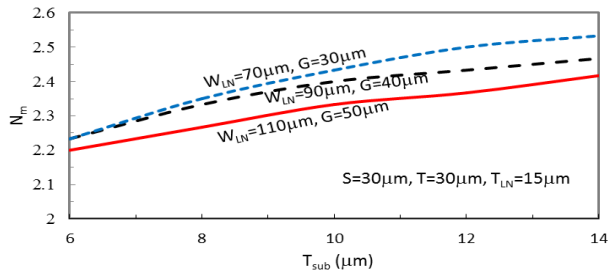
Fig. 8. The dependence of N_m on T_{sub}.

Fig. 9 shows the variation of the microwave characteristic impedance (Z_c in Ω) for the backside slot LN modulator with the substrate thickness (T_{sub} in μm). The obtained results agree very well with both theoretical and experimental results of [12]. The characteristic impedance decreases with the increase in substrate thickness.
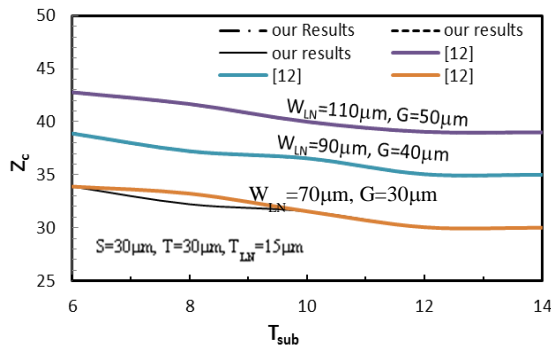

Fig. 9. Z_c as a function of T_{sub}.

Finally, Fig. 10 indicates the dependence of the bandwidth on the substrate thickness. The plotted curves show the bandwidth of the backside slot LN modulator when both conductor and the dielectric loss are taken into consideration. In this case, the value of optical effective index N_o and the length of the modulator L are taken as 2.15 and 2.7cm, respectively. From Fig. 10, one can notice that the highest value of bandwidth for this type of modulator is significantly affected by the gap width. The highest value as 80 GHz can be achieved when conductor and the dielectric loss are considered.
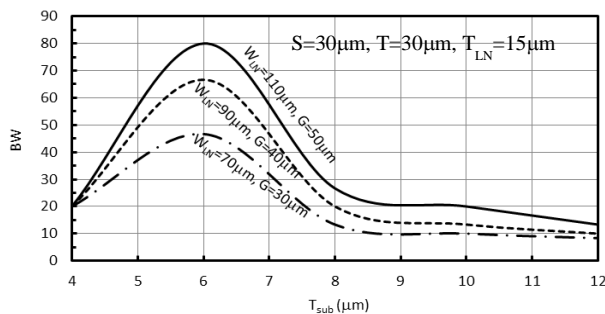

Fig. 10. 3dB optical BW as a function of T_{sub}.

5. Conclusions

A numerical model of x-cut LiNbO3 optical modulator with a two step back slot and backside slot structures was presented. The analysis was based on the transverse resonance technique. The effects of the space between the two steps W, the thickness T_{sub} near the ground electrodes and the gap G were examined. The numerical results show that, the modulator structure can satisfy the condition of velocity matching in the 50 Ω impedance system without the SiO2 buffer layer. Thus, the modulator gives a lower drive voltage V_π and a lower optical insertion loss. The dc-drift phenomenon due to the buffer layer can be eliminated. It is found from the results that the optical 3 dB bandwidth reaches about 25 GHz. The performance of this modulator is more sufficient for the 40 Gb/s optical transmission systems. For the backside slot structure, the highest value as 80 GHz can be achieved when conductor and the dielectric loss are considered.

References

[1] K. Noguchi, et al., IEICE Trans. Electron., (8), 1316 (1998).

[2] W. K. Burns, et al., J. Lightwave Technol., **17**(12), 2551 (1999).

[3] R. Madabhushi, et al., ECOC'98, Tech. Dig., Madrid, Spain, 547 (1998).

[4] H. Miyazawa, et al., "DC drift phenomena of LiNbO3 optical modulator," in Proc. IEICE'94, Paper SA-9-3(1994).

[5] S. K. Korotky, J. J. Veselka, J. Lightwave Technol., **14**, 2687 (1996).

[6] H. Nagata, IEEE Photonics Technol. Lett., **12**(11), 1477 (2000).

[7] P. Hallemeler, et al., Proc. NFOEC'99, Chicago, IL, USA, 26 (1999).

[8] M. Minakata, M. Goto, JICAST'98/CPST'98, Conf. Pub., Japan (1998).

[9] J. Kondo et al., Electron. Lett., **38**(10), May (2002).

[10] Ahmed A. Abou El-Fadl, A. Zarea, O. M. Ba-Rukab, CCECE 2000, World Trade and Convention Center, Halifax, Nova Scotia, Canada, May 7-10, (2000).

[11] Ahmed A. Abou El-Fadl, K. A. Mostafa, T. E. Taha, A. A. Aboul-Enien, *NRSC'2001,* D7(2001).

[12] M. Shah Alam, M. Khaled Hassan, M. Sakawat Ali, Proc. of the International Conference on Computer and Communication Engineering, Kuala Lumpur, Malaysia, May 13-15(2008).

[*]Corresponding author: ahmed251056@yahoo.com